JASA ARTICLE

Scattering by a rigid sphere of audio sound generated by a parametric array loudspeaker

Jiaxin Zhong,[1,a)] Ray Kirby,[1,b)] Mahmoud Karimi,[1,c)] Haishan Zou,[2,d)] and Xiaojun Qiu[2,e)]
[1]*Centre for Audio, Acoustics and Vibration, University of Technology Sydney, New South Wales 2007, Australia*
[2]*Key Laboratory of Modern Acoustics and Institute of Acoustics, Nanjing University, Nanjing 210093, China*

ABSTRACT:
This work investigates the scattering by a rigid sphere of audio sound generated by a parametric array loudspeaker (PAL). A computationally efficient method utilizing a spherical harmonic expansion is developed to calculate the quasilinear solution of audio sound fields based on both Kuznetsov and Westervelt equations. The accuracy of using the Westervelt equation is examined, and the rigid sphere scattering effects are simulated with the proposed method. It is found the results obtained using the Westervelt equation are inaccurate near the sphere at low frequencies. Contrary to conventional loudspeakers, the directivity of the audio sound generated by a PAL severely deteriorates behind a sphere, as the ultrasounds maintaining the directivity of the audio sound are almost completely blocked by the sphere. Instead, the ultrasounds are reflected and generate audio sound on the front side of the sphere. It means that a listener in front of the PAL will hear the audio sound scattered back after introducing the sphere as if it is reflected by the sphere. The experiment results are also presented to validate the numerical results.
 https://doi.org/10.1121/10.0009750
(Received 13 August 2021; revised 11 December 2021; accepted 14 February 2022; published online 10 March 2022)
[Editor: James F. Lynch] Pages: 1615–1626

I. INTRODUCTION

The parametric array loudspeakers (PAL) are known for their capability of generating highly directional audio sound with the carrier wave of ultrasound.[1] It has been widely used in many scenarios including directional communications,[2] active noise control,[3] sound reproduction,[4] sound absorption measurements,[5] constructions of omni-directional sources,[6] and so on. It is common in some applications for a human to be inside the audible region, which causes scattering of the sound generated by a PAL.[2,7] Both the head and torso account for the scattering effect, but the head is the most important part because the ears are on it and only a little sound is incident on the torso when the highly directional beams are generated by a PAL. To investigate this effect, a human head can be approximately modeled as a rigid sphere and its interaction with audio sound generated by conventional loudspeakers have been well studied.[8,9] The effects of a sphere on the audio sound generated by a PAL are however different because the sound originates from the nonlinear interactions of waves.

When a PAL generates two intensive ultrasound beams at different frequencies, the difference-frequency wave (DFW, the audio sound) is generated due to the nonlinear interactions of ultrasound beams.[10] The generation of the DFW is complicated and some approximations and simplifications are usually assumed in the mathematical modelling.[11–13] The fundamental governing equation is the second-order nonlinear wave equation, which is obtained by ignoring the terms of cubic and higher order in the acoustic variables.[12] The accuracy of the equation has been examined by researchers.[14] One of its equivalent forms is called the Kuznetsov equation and this is expressed in terms of the velocity potential instead of acoustic pressure.[12,13] If the Lagrangian density in the second-order nonlinear wave equation is neglected, it may then be simplified to give the Westervelt equation. This equation can be further reduced to the well-known Khokhlov-Zabolotskaya-Kuznetsov (KZK) equation by assuming the paraxial approximation for both ultrasonic and audio waves.[11,15] Because the ultrasound level generated by a PAL is limited, the nonlinearity is weak, and so the quasilinear approximation can be safely made to simplify calculations based on the governing equations.

The prediction of audio sound generated by a PAL in a free field has been extensively studied.[11,16–18] Recently, it was proposed that the audio sound field can be divided into three regions: the near field, the Westervelt far field, and the inverse-law far field.[11] In the near field close to the radiation surface, the local effects characterized by the Lagrangian density are significant so that the second-order nonlinear wave equation is required in the modelling. However, the Kuznetsov equation is more convenient because one can avoid the evaluation of the second order spatial derivatives of the ultrasonic Lagrangian density. In the Westervelt far field, the local effects are negligible and the Westervelt equation is accurate enough to use. In the inverse-law far field, the audio sound pressure is inversely proportional to

[a)]ORCID: 0000-0002-9972-8004.
[b)]ORCID: 0000-0002-3520-1377.
[c)]ORCID: 0000-0002-2949-5364.
[d)]Electronic mail: hszou@nju.edu.cn
[e)]ORCID: 0000-0002-5181-1220.

the propagating distance and much simpler solutions can be obtained.[19] There are also other well-established models for the reflection and transmission properties,[20,21] as well as a horned PAL,[13,22] the insertion of the acoustic lens,[23] and so on. However, there is a little research on the sphere scattering of audio sound generated by a PAL.

Based on the Westervelt equation and the quasilinear approximations, an analytic expression for the sound pressure of the DFW was obtained when primary plane waves interact with a rigid sphere.[24] This work showed that the total sound pressure of the DFW is a combination of nonlinear interactions from the incident primary waves (incident-with-incident) and the scattered primary waves (scattered-with-scattered), as well as the incident and scattered primary waves (incident-with-scattered). The solution is inaccurate because higher order spherical harmonics in the Green's function are neglected and the scattered waves do not follow the plane wave assumption. Furthermore, the accuracy of the Westervelt equation is not examined and the prediction error is large because the local effects near the sphere and between it and the PAL are significant. Although full spherical harmonics were considered in Ref. 25, the calculation was limited to the far field solution. The simulation was conducted for a small sphere with the radius of only 1.0 mm, which was insonified by two intersecting plane waves under the water. Therefore, the results and conclusions are likely to be different for a sphere with the size of a human head exposed to audio sound generated by a piston-like PAL in air. Besides, no detailed experiment results to support the accuracy of these respective studies have been reported to date.

In this paper, a computationally efficient method is developed to calculate the quasilinear solution of the audio sound generated by a PAL based on both the Kuznetsov and Westervelt equations. The ultrasound field generated by a circular piston is obtained first by using a spherical harmonic expansion. The audio field is then considered as the radiation from an infinitely large virtual volume source, with the source density proportional to the product of the ultrasonic pressure. The accuracy of the Westervelt equation is then examined and simulations of scattering by a rigid sphere are conducted. Results are compared to those for a conventional loudspeaker and experimental results are presented to validate these predictions.

II. THEORY

A circular PAL radiating towards a rigid sphere is shown in Fig. 1. Both the PAL and the sphere are assumed to be placed in a free field and the PAL is not baffled. The radii of the PAL and the sphere are denoted by a and r_0, respectively. To achieve maximum scattering effects, the center of the sphere is placed on the radiation axis of the loudspeaker. The distance between their centroids is denoted by d. A Cartesian coordinate system (x, y, z) is established with its origin, O, at the center of the sphere and the negative z axis pointing to the center of the PAL. The spherical coordinates (r, θ, φ) and the cylindrical coordinates (ρ, φ, z) are

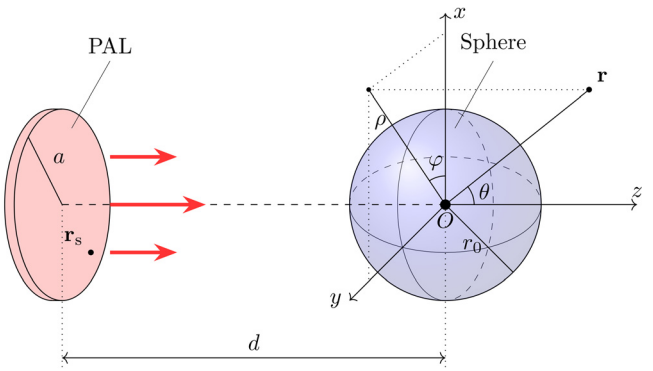

FIG. 1. (Color online) Sketch of a circular PAL near a sphere.

established with respect to the Cartesian coordinates (x, y, z) for further calculations, where r, θ, φ, and ρ are the radial distance, zenith angle, azimuth angle, and polar radial distance, respectively.

A. Governing equations and the quasilinear solutions

The propagation of waves generated by a PAL is governed by the second order nonlinear wave equation, after ignoring cubic and higher order terms in the acoustic variables. However, it is difficult to solve this equation because it requires the evaluation of the derivatives of Lagrangian density, which reads[11–13]

$$L = \frac{\rho_0 \mathbf{v}\cdot\mathbf{v}}{2} - \frac{p^2}{2\rho_0 c_0^2}, \tag{1}$$

where ρ_0 is the air density, c_0 is the linear sound speed, p is the acoustic pressure, and $\mathbf{v}$ is the particle velocity vector, which is related to the velocity potential, Φ, by $\mathbf{v} = \nabla\Phi$.

The Kuznetsov equation is equivalent to the second-order nonlinear wave equation but is expressed in terms of the velocity potential instead of acoustic pressure. It is used in this paper and reads[11–13]

$$\nabla^2\Phi - \frac{1}{c_0^2}\frac{\partial^2\Phi}{\partial t^2} + \frac{\delta}{c_0^2}\nabla^2\frac{\partial\Phi}{\partial t} = \frac{1}{c_0^2}\frac{\partial}{\partial t}\left[(\nabla\Phi)^2 + \frac{\beta-1}{c_0^2}\left(\frac{\partial\Phi}{\partial t}\right)^2\right], \tag{2}$$

where t is the time, β is the nonlinearity coefficient, and δ is the sound diffusivity which relates to the atmospheric sound attenuation coefficient α at the angular frequency ω by $\alpha(\omega) = \omega^2\delta/(2c_0^3)$.[26]

In the case of progressive plane waves, $L = 0$ so the second-order nonlinear wave equation reduces to the well-known Westervelt equation,[11,13]

$$\nabla^2 p - \frac{1}{c_0^2}\frac{\partial^2 p}{\partial t^2} + \frac{\delta}{c_0^2}\nabla^2\frac{\partial p}{\partial t} = -\frac{\beta}{\rho_0 c_0^4}\frac{\partial^2 p^2}{\partial t^2}. \tag{3}$$

This equation is usually used in the modelling of PAL radiation in a free field because it is easier to calculate and the ultrasound waves are well collimated.[16,17] It has been

https://doi.org/10.1121/10.0009750

demonstrated that the Lagrangian density cannot be neglected in the near field due to the complexity of the ultrasound field.[11,13,27] Since the scattered ultrasound field near the sphere does not behave like plane waves, it is necessary first to examine the accuracy of using Eq. (3) when predicting the audio sound near the sphere.

Assume the PAL generates two harmonic ultrasounds at frequencies f_1 and f_2 ($f_1 > f_2$), and the boundary condition on the transducer surface is

$$u(x,y,t) = u_1(x,y)\mathrm{e}^{-\mathrm{i}\omega_1 t} + u_2(x,y)\mathrm{e}^{-\mathrm{i}\omega_2 t}, \tag{4}$$

where i is the imaginary unit, u represents the vibration velocity normal to the transducer surface, u_i is the amplitude of the vibration velocity, $\omega_i = 2\pi f_i$ is the angular frequency of the i-th primary wave, and $i = 1, 2$. The solutions of the ultrasound and audio sound are denoted by

$$\tilde{p}_i(\mathbf{r},t) = p_i(\mathbf{r})\mathrm{e}^{-\mathrm{i}\omega_i t},\ i = 1, 2, \mathrm{a}, \tag{5}$$

where the subscripts "1", "2", and "a" represent the ultrasound and audio sound respectively, and $\mathbf{r} = (x, y, z)$ are the spatial coordinates.

After using the method of successive and quasilinear approximations in the frequency domain, Eq. (2) can be decomposed into two coupled linear equations. One is the homogeneous equation for the ultrasound and the other is the inhomogeneous equation for audio sound with the source term of[11,13]

$$q(\mathbf{r}) = \frac{\omega_\mathrm{a}}{\mathrm{i}c_0^2}\left[(\beta-1)\frac{\omega_1\omega_2}{c_0^2}\Phi_1(\mathbf{r})\Phi_2^*(\mathbf{r}) + \mathbf{v}_1(\mathbf{r})\cdot\mathbf{v}_2^*(\mathbf{r})\right], \tag{6}$$

where Φ_i and $\mathbf{v}_i$ are the velocity potentials and the velocity of the ultrasound at f_i, $i = 1$ and 2, and the superscript "*" represents the complex conjugate. The sound pressure of audio sound can be obtained using its second-order relationship with the velocity potential as[11,13]

$$p_\mathrm{a}(\mathbf{r}) = \mathrm{i}\rho_0\omega_\mathrm{a}\Phi_\mathrm{a}(\mathbf{r}) - \frac{\rho_0}{2}\mathbf{v}_1(\mathbf{r})\cdot\mathbf{v}_2^*(\mathbf{r}) + \frac{\rho_0\omega_1\omega_2}{2c_0^2}\Phi_1(\mathbf{r})\Phi_2^*(\mathbf{r}). \tag{7}$$

For the quasilinear solution using the Westervelt equation shown in Eq. (3), the source density in Eq. (6) and the relation in Eq. (7) are respectively simplified into

$$q(\mathbf{r}) = \frac{\beta\omega_\mathrm{a}\omega_1\omega_2}{\mathrm{i}c_0^4}\Phi_1(\mathbf{r})\Phi_2^*(\mathbf{r}), \tag{8}$$

and

$$p_\mathrm{a}(\mathbf{r}) = \mathrm{i}\rho_0\omega_\mathrm{a}\Phi_\mathrm{a}(\mathbf{r}). \tag{9}$$

B. Ultrasound field

A rigorous approach to modelling the ultrasound field should include scattering from both the non-baffled PAL and the sphere, as well as the interaction between them. It has been demonstrated in Ref. 16 that the ultrasound generated by a non-baffled PAL can be approximated by the one generated by a baffled PAL because the size of the PAL is large enough when compared to the wavelength of the ultrasound. The interaction between a PAL and a sphere is known to generate multiple scattering; however, when the separation between them is larger than the ultrasonic wavelength and the dimensions of each component, then this scattering is considered to be insignificant.[28] It is therefore neglected in this paper for simplicity and to focus on the scattering effects by the sphere.

The ultrasound pressure at a field point $\mathbf{r} = (r, \theta, \varphi)$ in the presence of a rigid sphere shown in Fig. 1 is solved using the Rayleigh integral,

$$\Phi_i(\mathbf{r}) = -2\iint_S u_i(\boldsymbol{\rho}_\mathrm{s})G(\mathbf{r},\mathbf{r}_\mathrm{s},k_i)\mathrm{d}^2\boldsymbol{\rho}_\mathrm{s},\quad r \geq r_0,\ i = 1,2, \tag{10}$$

where the variables $\boldsymbol{\rho}_\mathrm{s} = (\rho_\mathrm{s}, \varphi_\mathrm{s})$ are the polar coordinates for the area element on the PAL surface S, $\mathbf{r}_\mathrm{s} = (\rho_\mathrm{s}, \varphi_\mathrm{s}, z_\mathrm{s})$ are the cylindrical coordinates, and $z_\mathrm{s} = -d$. The Green's function $G(\mathbf{r},\mathbf{r}_\mathrm{s},k_i)$ is the velocity potential solution at the field point $\mathbf{r}$ generated by a point monopole at $\mathbf{r}_\mathrm{s}$ with the unit volume velocity and wavenumber $k_i = \omega_i/c_0 + \mathrm{i}\alpha_i$,[29–31]

$$G(\mathbf{r},\mathbf{r}_\mathrm{s},k_i) = \frac{\mathrm{i}k_i}{4\pi}\sum_{n=0}^{\infty}(2n+1)R_n(r,r_\mathrm{s},k_i) \times \sum_{m=-n}^{n}\frac{(n-m)!}{(n+m)!}P_n^m(\cos\theta) \times P_n^m(\cos\theta_\mathrm{s})\mathrm{e}^{\mathrm{i}m(\varphi-\varphi_\mathrm{s})}, \tag{11}$$

where α_i is the sound absorption coefficient at f_i,[26] and the radial component

$$R_n(r,r_\mathrm{s},k_i) = h_n(k_i r_{\mathrm{s},>})j_n(k_i r_{\mathrm{s},<}) - \frac{j_n'(k_i r_0)}{h_n'(k_i r_0)} \times h_n(k_i r)h_n(k_i r_\mathrm{s}), \tag{12}$$

$r_{\mathrm{s},>} = \max(r, r_\mathrm{s})$, $r_{\mathrm{s},<} = \min(r, r_\mathrm{s})$, $P_n^m(\cos\theta)$ is the associated Legendre function of order m and degree n, where $j_n(k_i r_0)$ and $h_n(k_i r_0)$ are the spherical Bessel and Hankel functions, respectively, and the apostrophe denotes the derivatives with respect to the functions' argument. Equation (11) represents the spherical wave expansion of the Green's function for a point source located near a rigid sphere in the free field. The rigid boundary condition on the spherical surface, $\partial G/\partial r|_{r=r_0} = 0$, can be verified by taking the derivative of Eq. (12) with respect to r.

In this paper, the velocity profile for the ultrasound on the PAL surface is assumed to be axisymmetric for simplicity, that is $u_i(\boldsymbol{\rho}_\mathrm{s}) = u_i(\rho_\mathrm{s})$. Equation (10) is then rewritten as

$$\Phi_i(\mathbf{r}) = \frac{1}{\mathrm{i}k_i}\sum_{n=0}^{\infty}(2n+1)\sum_{m=-n}^{n}\frac{(n-m)!}{(n+m)!}P_n^m(\cos\theta) \times\left[\frac{1}{2\pi}\int_0^{2\pi}\mathrm{e}^{\mathrm{i}m(\varphi-\varphi_\mathrm{s})}\mathrm{d}\varphi_\mathrm{s}\right] \times\left[\int_0^a u_i(\rho_\mathrm{s})R_n(r,r_\mathrm{s},k_i)P_n^m(\cos\theta_\mathrm{s})k_i^2\rho_\mathrm{s}\mathrm{d}\rho_\mathrm{s}\right],\quad r\geq r_0, \tag{13}$$

with the following relations:

$$\begin{cases} r_\mathrm{s}^2=\rho_\mathrm{s}^2+d^2\Rightarrow r_\mathrm{s}\mathrm{d}r_\mathrm{s}=\rho_\mathrm{s}\mathrm{d}\rho_\mathrm{s} \\ \cos(\pi-\theta_\mathrm{s})=\dfrac{d}{r_\mathrm{s}}. \end{cases} \tag{14}$$

By substituting Eq. (14) into Eq. (13) and using the fact that the integral with respect to φ_s is non-zero when $m=0$, and the symmetry relation of the Legendre polynomials [see Eq. (4.2.8) in Ref. 32],

$$P_n(\cos\theta_\mathrm{s})=P_n\left(-\frac{d}{r_\mathrm{s}}\right)=(-1)^nP_n\left(\frac{d}{r_\mathrm{s}}\right), \tag{15}$$

one obtains

$$\Phi_i(\mathbf{r})=\frac{1}{\mathrm{i}k_i}\sum_{n=0}^{\infty}(-1)^n(2n+1)P_n(\cos\theta)\chi_n(r,k_i),\quad r\geq r_0, \tag{16}$$

where the radial component χ_n is

$$\chi_n(r,k_i)=\int_d^{\sqrt{d^2+a^2}}u_i(\rho_\mathrm{s})R_n(r,r_\mathrm{s},k_i)P_n\left(\frac{d}{r_\mathrm{s}}\right)k_i^2r_\mathrm{s}\mathrm{d}r_\mathrm{s}. \tag{17}$$

Compared to the Rayleigh integral in Eq. (10), Eq. (16) is much more efficient to calculate because the convergence of the series is faster than a double integral and the field coordinates are also independent.[33,34] The components of the particle velocity of the ultrasound under the spherical coordinate system is then obtained from Eq. (16) to give

$$\begin{cases} v_{i,r}(\mathbf{r})=\dfrac{\partial\Phi_i(\mathbf{r})}{\partial r} \\ \quad=\dfrac{1}{\mathrm{i}}\displaystyle\sum_{n=0}^{\infty}(-1)^n(2n+1)P_n(\cos\theta)\frac{\mathrm{d}\chi_n(r,k_i)}{\mathrm{d}(k_ir)} \\ v_{i,\theta}(\mathbf{r})=\dfrac{1}{r}\dfrac{\partial\Phi_i(\mathbf{r})}{\partial\theta} \\ \quad=\dfrac{1}{\mathrm{i}}\displaystyle\sum_{n=0}^{\infty}(-1)^n(2n+1)\frac{\mathrm{d}P_n(\cos\theta)}{\mathrm{d}\theta}\frac{\chi_n(r,k_i)}{k_ir} \\ v_{i,\varphi}(\mathbf{r})=\dfrac{1}{r\sin\theta}\dfrac{\partial\Phi_i(\mathbf{r})}{\partial\varphi}=0. \end{cases} \tag{18}$$

C. Audio sound field

The velocity potential of audio sound is governed by an inhomogeneous Helmholtz equation with the source density of Eq. (6). It can be treated as the superposition of sound produced by infinite number of virtual point sources at $\mathbf{r}_\mathrm{v}=(r_\mathrm{v},\ \theta_\mathrm{v},\ \varphi_\mathrm{v})$ with the source density function $q(\mathbf{r}_\mathrm{v})$.[18] Therefore, this equation can be solved by integrating the source density using the Green's function with spherical scattering,

$$\Phi_\mathrm{a}(\mathbf{r})=-\iiint_{r_\mathrm{v}\geq r_0}q(\mathbf{r}_\mathrm{v})G(\mathbf{r},\mathbf{r}_\mathrm{v},k_\mathrm{a})\mathrm{d}^3\mathbf{r}_\mathrm{v},\quad r\geq r_0, \tag{19}$$

where $k_\mathrm{a}=\omega_\mathrm{a}/c_0+\mathrm{i}\alpha_\mathrm{a}$ is the wavenumber of the audio sound.

For a circular PAL with a radius of a and an axisymmetric vibration velocity profile, the source density is not related to the azimuthal angle, so the triple integral of audio sound Eq. (19) can be simplified to give

$$\Phi_\mathrm{a}(\mathbf{r})=\frac{1}{\mathrm{i}k_\mathrm{a}^2}\sum_{n=0}^{\infty}\left(n+\frac{1}{2}\right)\sum_{m=-n}^{n}\frac{(n-m)!}{(n+m)!}P_n^m(\cos\theta) \times\left[\frac{1}{2\pi}\int_0^{2\pi}\mathrm{e}^{\mathrm{i}m(\varphi-\varphi_\mathrm{v})}\mathrm{d}\varphi_\mathrm{v}\right] \times\int_{r_0}^{\infty}\int_0^{\pi}q(\mathbf{r}_\mathrm{v})R_n(r,r_\mathrm{v},k_\mathrm{a})P_n^m(\cos\theta_\mathrm{v}) \times k_\mathrm{a}^3r_\mathrm{v}^2\sin\theta_\mathrm{v}\mathrm{d}\theta_\mathrm{v}\mathrm{d}r_\mathrm{v},\quad r\geq r_0. \tag{20}$$

Similar to Eq. (13), the integral with respect to φ_v is non-zero when $m=0$, and Eq. (20) then reduces to

$$\Phi_\mathrm{a}(\mathbf{r})=\frac{1}{\mathrm{i}k_\mathrm{a}^2}\sum_{n=0}^{\infty}\left(n+\frac{1}{2}\right)P_n(\cos\theta) \times\int_{r_0}^{\infty}\int_0^{\pi}q(\mathbf{r}_\mathrm{v})R_n(r,r_\mathrm{v},k_\mathrm{a})P_n(\cos\theta_\mathrm{v}) \times k_\mathrm{a}^3r_\mathrm{v}^2\sin\theta_\mathrm{v}\mathrm{d}\theta_\mathrm{v}\mathrm{d}r_\mathrm{v},\quad r\geq r_0. \tag{21}$$

D. Normalized spherical Bessel functions

The series in Eqs. (16) and (21) were found to require at least 1000 terms to deliver satisfactory convergence. In this paper, 2000 terms are chosen, and it has been confirmed the error of the calculation of the sound pressure level is less than 0.1 dB. This is because the wavelength of the ultrasound is much smaller than the size of the PAL as well as the sphere and the separation between them. However, spherical Bessel and Hankel functions are known to overflow and/or underflow (exceeding the range of the floating point used in the computer) for orders much larger than the argument.[35] To overcome this problem, normalized spherical Bessel and Hankel functions are used in this paper, which are related to the unnormalized ones as[35]

$$\begin{cases} \bar{j}_n(z_\mathrm{j})=\dfrac{(2n+1)!!}{z_\mathrm{j}^n}j_n(z_\mathrm{j}) \\ \bar{h}_n(z_\mathrm{h})=\dfrac{\mathrm{i}z_\mathrm{h}^{n+1}}{(2n-1)!!}h_n(z_\mathrm{h}), \end{cases} \tag{22}$$

https://doi.org/10.1121/10.0009750

where !! denotes a double factorial. MATLAB® was used for the computations of the normalized spherical Bessel and Hankel functions, see the algorithm in Ref. 35.

By using the relations Eq. (22) and Eq. (8.1.27) in Ref. 32, the following relations are also obtained:

$$j_n(z_j)h_n(z_h) = \frac{1}{i(2n+1)}\frac{z_j^n}{z_h^{n+1}}\bar{j}_n(z_j)\bar{h}_n(z_h), \tag{23}$$

$$j_n'(z_j)h_n(z_h) = \frac{z_j^{n-1}}{i(2n+1)z_h^{n+1}}\bar{h}_n(z_h) \times \left[n\bar{j}_n(z_j) - \frac{z_j^2}{2n+3}\bar{j}_{n+1}(z_j)\right], \tag{24}$$

$$j_n(z_j)h_n'(z_h) = \frac{z_j^n}{iz_h^{n+2}}\bar{j}_n(z_j)\left[\frac{n}{2n+1}\bar{h}_n(z_h) - \bar{h}_{n+1}(z_h)\right], \tag{25}$$

$$\frac{j_n'(z_d)}{j_n(z_0)} = \frac{z_d^{n-1}}{z_0^n\bar{j}_n(z_0)}\left[n\bar{j}_n(z_d) - \frac{z_d^2}{2n+3}\bar{j}_{n+1}(z_d)\right], \tag{26}$$

and

$$\frac{h_n'(z_d)}{h_n(z_0)} = \frac{z_0^{n+1}}{z_d^{n+2}\bar{h}_n(z_0)}[n\bar{h}_n(z_d) - (2n+1)\bar{h}_{n+1}(z_d)] \tag{27}$$

It is found in the simulations that the computations of the spherical Bessel and Hankel functions using these relations do not overflow and/or underflow when the orders are up to 10^4 for the parameters used in this paper.

III. SIMULATIONS

Numerical simulations are conducted here using MATLAB R2020b. The center frequency of the ultrasound,

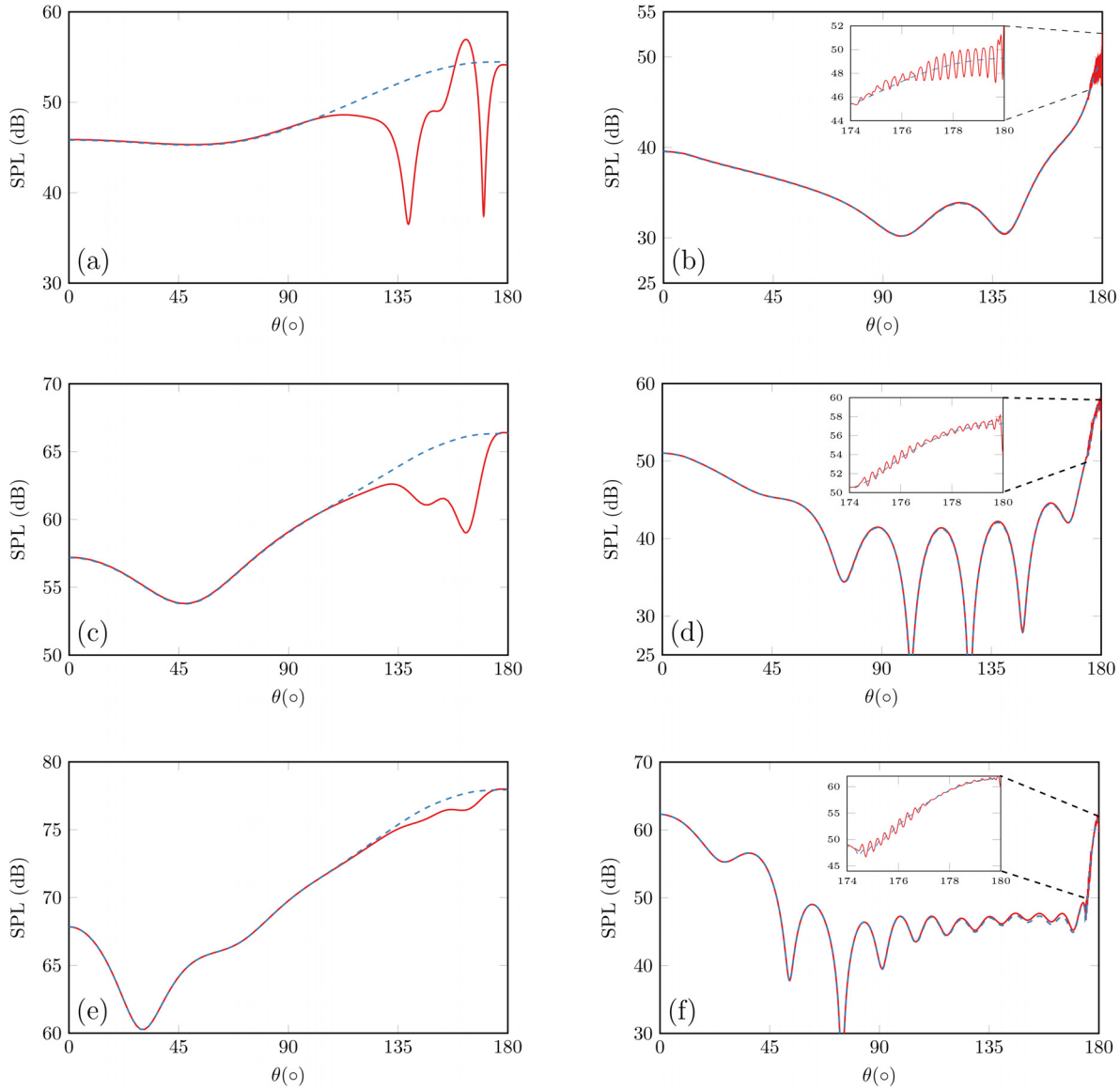

FIG. 2. (Color online) Audio sound at the different zenith angles with the distance of $d = 0.1$ m (left column) and $d = 1$ m (right column) to the center of the sphere generated by a PAL at: (a), (b) 500 Hz, (c), (d) 1 kHz, and (e) and (f) 2 kHz. Solid line, Kuznetsov equation; dashed line, Westervelt equation.

i.e., $f_u = (f_1 + f_2)/2$, is set as $f_u = 64$ kHz, which is a common value used in commercial PALs. The sound attenuation coefficient, α_u, at 64 kHz is approximately 0.3 Np/m calculated according to ISO 9613-1 with the relative humidity 60% and temperature 25 °C.[36] The radii of the PAL and the sphere are both set as 0.1 m. The Rayleigh distance is therefore 5.86 m, which can be calculated by $k_u a^2/2$, where k_u is the ultrasonic wavenumber at the frequency of f_u. The distance between the PAL and the sphere, d, is set as 1.0 m. The double integral presented in Eq. (21) is computed using Gauss-Legendre quadrature. The upper limit of the integration interval for the radial coordinate, r_v, is truncated to 5 m. This truncation results in no significant loss of accuracy because the virtual source density is attenuated by more than 13 dB when $r_v > 5$ m, which is calculated by $20\log_{10}[\exp(5\alpha_u)] \approx 13$ dB. The audio sound fields generated by a PAL without the sphere are obtained using the spherical harmonic expansion method in Refs. 11 and 18. The audio sound fields generated by a conventional loudspeaker with and without the sphere are calculated by setting k_a in Eq. (16) and using the method described in Ref. 34, respectively. A uniform vibration velocity profile is assumed for all cases and an amplitude of 0.12 m/s and 2.0×10^{-4} m/s are set for the ultrasounds generated by the PAL and the

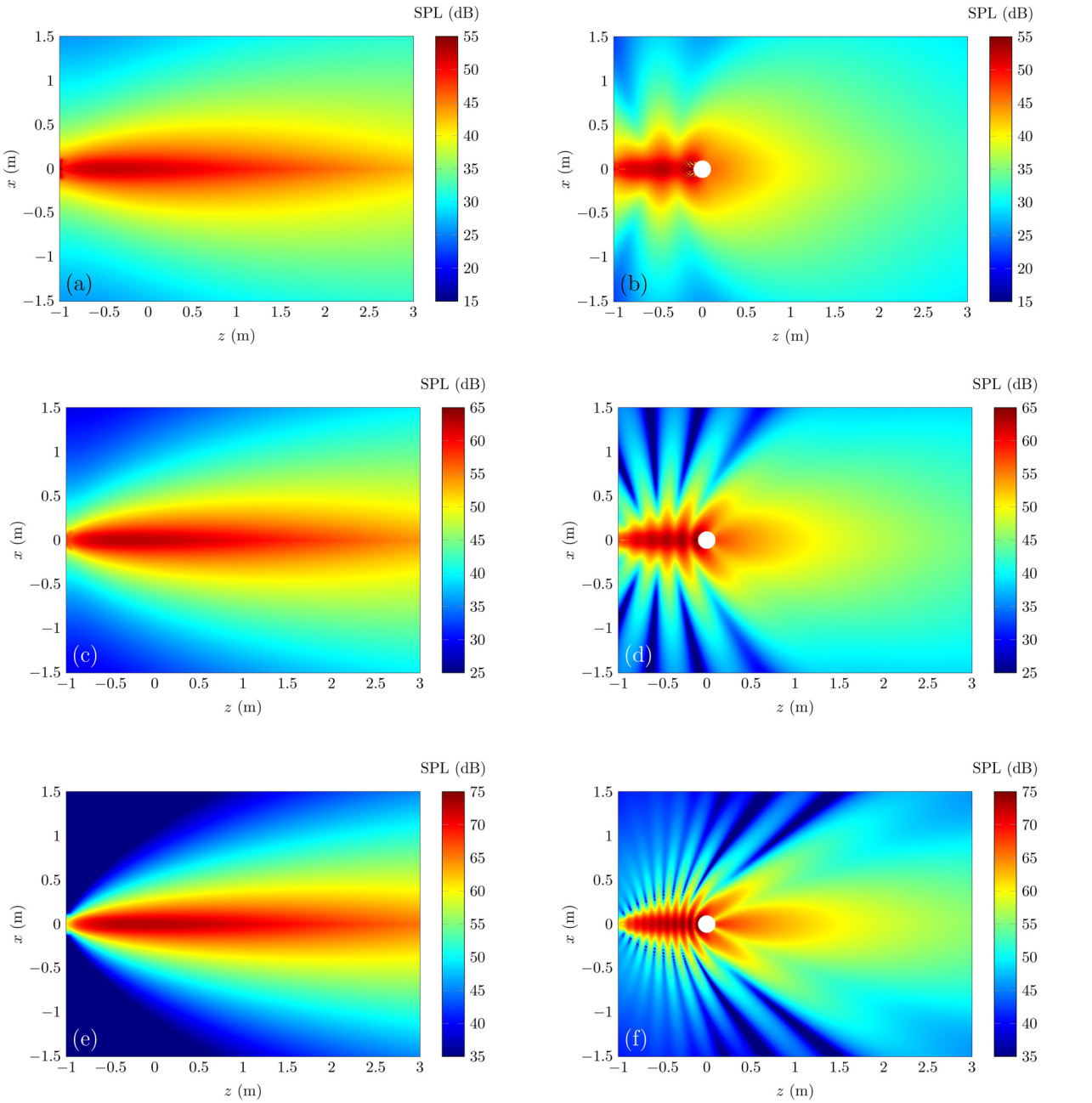

FIG. 3. (Color online) Sound fields generated by a PAL without the sphere (left column) and with the sphere (right column) at (a), (b), 500 Hz, (c), (d), 1 kHz, and (e) and (f) 2 kHz.

https://doi.org/10.1121/10.0009750

audio sound generated by the conventional loudspeaker, respectively. The reference quantity for the sound pressure level (SPL) used in the following text is 20 μPa.

A. The accuracy of the Westervelt equation

Figure 2 compares the SPL for audio sound generated by a PAL using the Westervelt and Kuznetsov equations at different zenith angles, θ, with a distance of 0.1 m or 1.0 m to the center of the sphere at 500 Hz, 1 kHz, and 2 kHz. Figure 2 shows that the audio SPL calculated with the Kuznetsov equation differs from that obtained using the Westervelt equation, which is also observed for the case without the sphere.[11,13] The difference between the SPLs calculated using these two equations is large when the observation point is close to the sphere or the PAL. For example at the angle $\theta = 170°$, when the distance between the field point and the center of the sphere is 0.1 m, the difference of SPLs is 16.5, 2.6, and 0.5 dB at 500 Hz, 1 kHz, and 2 kHz, respectively. When the distance is 1.0 m, fluctuations can be observed when the zenith angle approaches to 180° and they are comparable to the ultrasonic wavelength of 5.4 mm at 64 kHz. The reason is that the ultrasonic field is complicated and the pressure is large near the sphere and the PAL indicating that the local effects are strong, which cannot be correctly captured by the Westervelt equation.

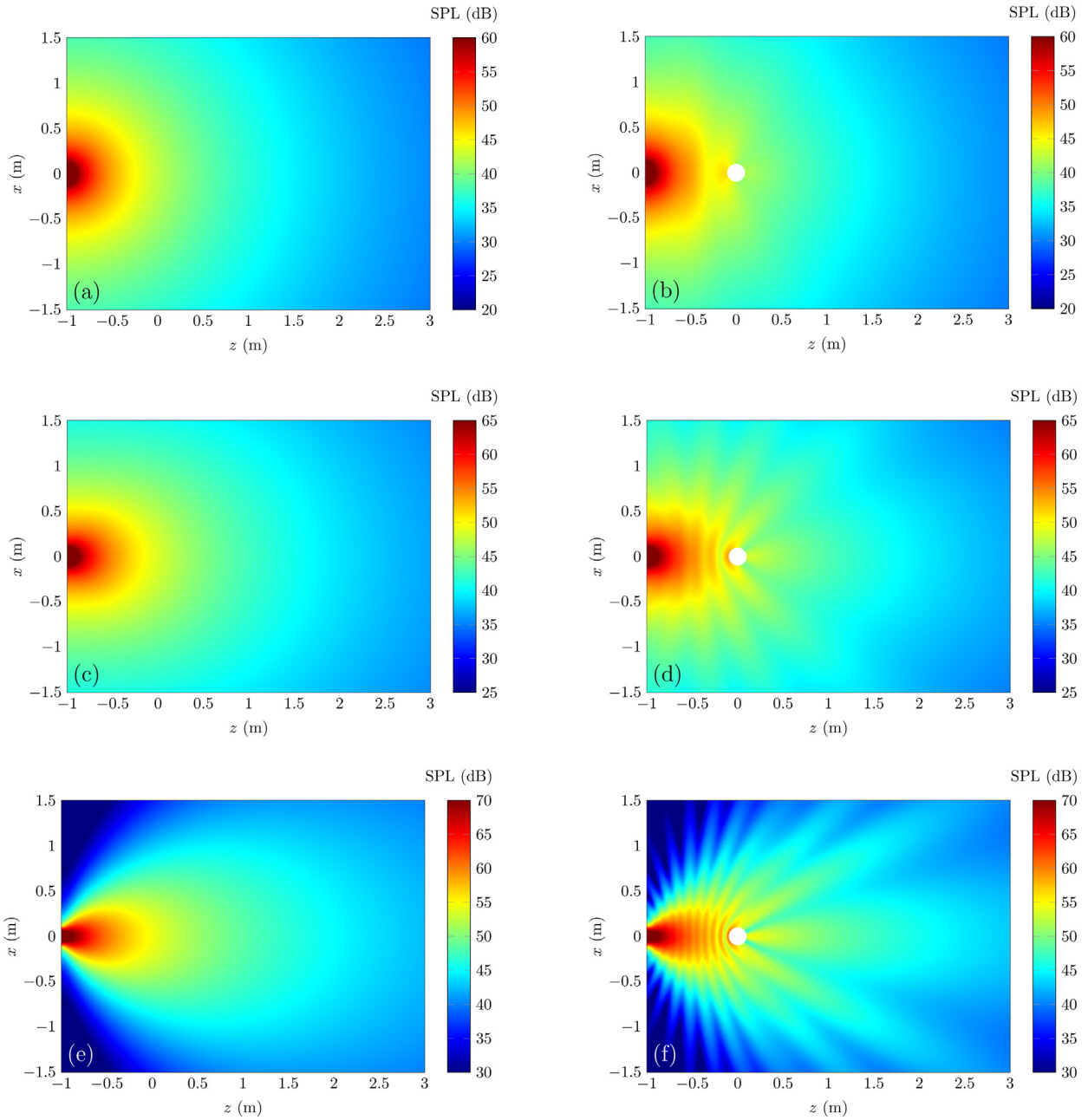

FIG. 4. (Color online) Sound fields generated by a conventional loudspeaker without the sphere (left column) and with the sphere (right column) at (a), (b) 500 Hz, (c), (d), 1 kHz, and (e), (f) 2 kHz.

The difference between the SPLs using these two equations becomes smaller as the frequency increases. This is because the audio SPL calculated with the Westervelt equation increases by about 12 dB when the audio frequency is doubled, but corresponding changes in the amplitude of the ultrasonic Lagrangian density are relatively small, so its effect on the audio SPL is small at high audio frequencies. Therefore, it is concluded that the Kuznetsov equation should be used in the calculation, especially for observation points near the sphere and the PAL at low frequencies. Accordingly, all the simulations that follow are obtained using the Kuznetsov equation.

B. Scattering effects by a rigid sphere

The audio sound fields generated by a PAL with and without the sphere at 500 Hz, 1 kHz, and 2 kHz are shown in Fig. 3. For comparison, the sound fields generated by a conventional loudspeaker with the same size as that of the PAL are presented in Fig. 4. Because the generated SPL is increased by 12 and 6 dB, respectively, for the PAL and conventional loudspeaker when the frequency is doubled, the range of the color bar in Figs. 3 and 4 is increased by 10 and 5 dB as frequency is doubled for better comparison. Compared to the conventional loudspeaker, the directivity of the audio sound generated by the PAL is seen to be more focused. After introducing the sphere, the scattering effects become progressively more significant as the frequency increases for both the PAL and the conventional loudspeaker. This is because the audio sound wavelength becomes smaller compared to the sphere and so more audio sound is reflected at higher frequencies. For the conventional loudspeaker, the effects of the sphere on the back side ($z > 0$) are negligible at low frequencies because the audio wavelength

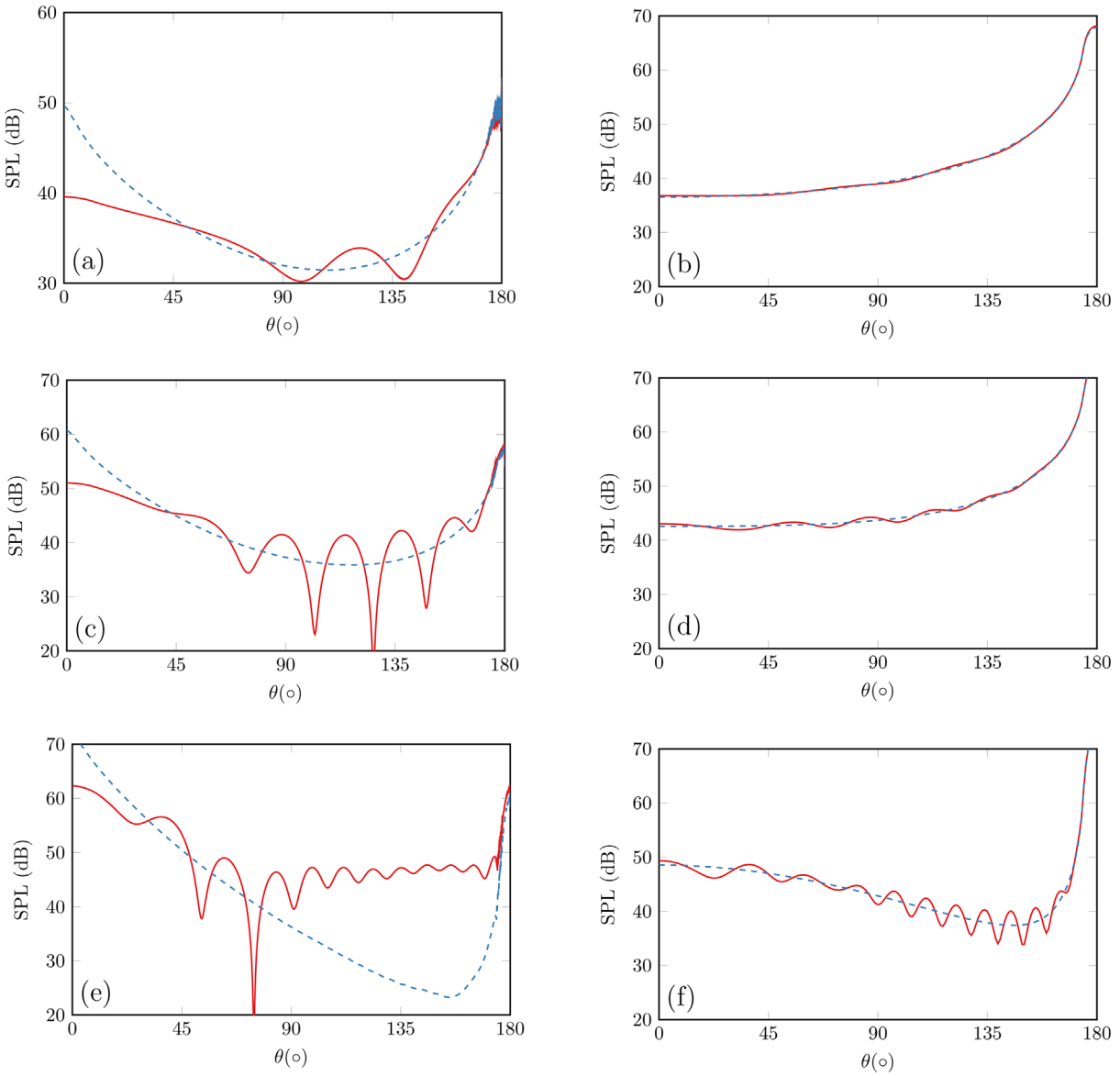

FIG. 5. (Color online) Audio sound at the different zenith angles with a distance of 1.0 m to the center of the sphere generated by a PAL for (a), (c), and (e) and a conventional loudspeaker for (b), (d), and (f) with and without the sphere at 500 Hz for (a) and (b), 1 kHz for (c) and (d), and 2 kHz for (e) and (f). Solid line, with sphere; dashed line, without sphere.

https://doi.org/10.1121/10.0009750

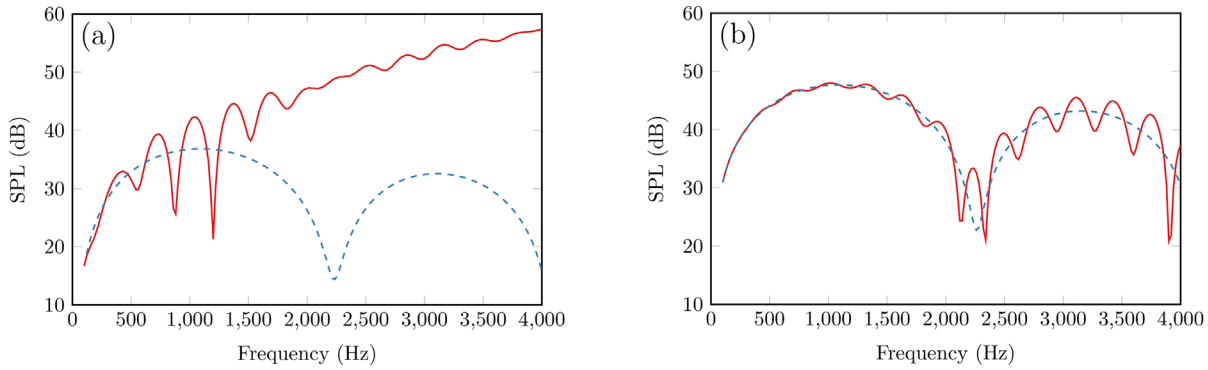

FIG. 6. (Color online) Audio sound at the zenith angle $\theta = 135°$ and the radius of 1.0 m generated by (a) a PAL and (b) a traditional loudspeaker from 100 Hz to 4 kHz. Solid line, with sphere; dashed line, without sphere.

is much larger than the size of the sphere.[8] However, the SPL on the back side of a sphere generated by a PAL decreases significantly because the audio beams are no longer highly collimated.

Figure 5 shows the SPL at different zenith angles, θ, with a distance of 1.0 m to the center of the sphere generated by a PAL or a conventional loudspeaker with and without the sphere. After introducing the sphere, the half sound pressure (-6 dB) angles for the audio sound generated by the PAL are increased from 15.9°, 13.1°, and 10.8° to 76.4°, 50.2°, and 21.8° at 500 Hz, 1 kHz, and 2 kHz, respectively, while there is little change observed for the conventional loudspeaker. This demonstrates that the sphere severely deteriorates the directivity of the audio sound generated by a PAL, because the ultrasounds maintaining the directivity of the audio sound are almost completely blocked by the sphere.

It is interesting to note that the audio sound generated by the PAL are augmented at some angles and frequencies on the front side ($z < 0$) after introducing the sphere, while the SPL changes a little for the case with the conventional loudspeaker. For example, the SPL at the zenith angle of 135° increases from 36.7 and 25.7 dB to 41.7 and 47.2 dB at 1 and 2 kHz, respectively. Figure 6 compares the SPL at the zenith angle of 135° with and without the sphere, for both the PAL and the conventional loudspeaker, at different frequencies. The difference of the SPL with and without the sphere fluctuates for the conventional loudspeaker and the fluctuation becomes larger as the frequency increases. The increment of the SPL is no larger than 6 dB below 4 kHz for the conventional loudspeaker. However, the SPL is generally enlarged after introducing the sphere, as the frequency increases for the audio sound generated by the PAL. The increment of the SPL is more than 6 dB at frequencies larger than 1620 Hz. This means that a listener outside the audible region of the PAL can still hear a significant augmentation of the audio sound when a human head moves across the radiation direction of the PAL. The reason is that the ultrasounds are almost completely reflected from the sphere because their wavelength is much smaller than the sphere radius. The reflected ultrasounds form another virtual array which augments the audio sound on the front side of the sphere.

IV. EXPERIMENTS

The experiments were conducted in the hemi-anechoic room in University of Technology Sydney with dimensions of 7.2 m × 5.19 m × 6.77 m (height). The sketch and photos of the experimental setup are shown in Figs. 7 and 8, respectively. The sound field generated by a PAL with and without the sphere was measured in the experiments. A solid wooden sphere with a radius of 0.1 m and density of 1.2×10^3 kg/m^3 was used, and height of both the loudspeaker and sphere are 1.8 m. The wooden sphere was supported by a tripod, which was covered by absorption materials to avoid additional scattering effects from the tripod.

The PAL in the experiments is a Holosonics Audio Spotlight AS-24i with a surface size of 60 cm × 60 cm. The carrier frequency of the PAL is 64 kHz. The radiating surface of the PAL is covered by a 6 mm thick perspex panel with a hole of 10 cm radius at its center, as shown in Fig. 8(a). It has been demonstrated that the sound pressure levels on the radiation axis of the PAL decrease by more than 30 dB at 1 kHz when the PAL is covered by this perspex panel, which indicates that the panel successfully reproduces a circular piston source with a hole at the center.[21]

The sound field was measured in a 2.95 m × 4 m rectangular plane at the same height as the loudspeaker ($x = 0$ m, -1.45 m $\le y \le 1.5$ m, -1 m $\le z \le 3$ m). Sixty measurement

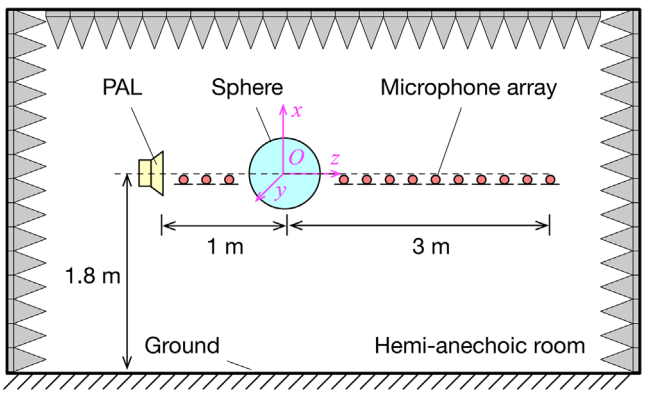

FIG. 7. (Color online) Front view of the experiment setup.

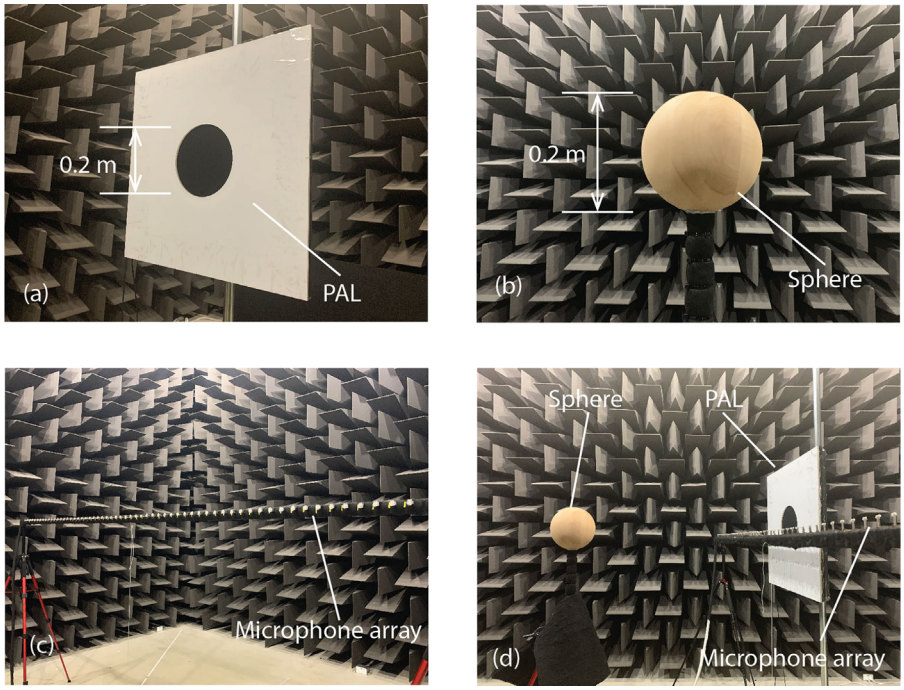

FIG. 8. (Color online) Photos of the experiment setup: (a) a PAL; (b) a solid wooden sphere; (c) a 60-channel microphone array; (d) the measurement system.

positions were taken in the y direction from $y=-1.45$ m to $y=1.5$ m with a spacing of 5 cm. The SPLs were measured simultaneously using a 60-channel microphone array, see Fig. 8(c). The microphone array was moved along the z-axis with a step of 10 cm to obtain the sound fields in the measurement plane.

All the measurement microphones are Brüel & Kjær type 4957 calibrated with a Brüel & Kjær 4231 calibrator and the sound pressure at microphones was sampled with a Brüel & Kjær PULSE system (the analyzer 3053-B-120 equipped with the front panel UA-2107–120). The fast Fourier transform (FFT) analyzer in PULSE LabShop was used to obtain the FFT spectrum. The frequency span was set to 6.4 kHz, with 6400 lines and the averaging type is linear with 66.67% overlap and 30 s duration. To avoid spurious sound at the microphones induced by the intensive ultrasounds radiated by the PAL,[37] all microphones were covered by a piece of small and thin plastic film. The experiment results (not presented here) show the insertion loss of this plastic film is more than 35 dB at 64 kHz and about 0.6 dB at 1 kHz. The relative humidity and temperature were 70% and 25.4 °C, respectively.

Figure 9 shows the measured results of the audio sound generated by a PAL with and without the sphere. Values close to the sphere cannot be measured and so they are left blank in Figs. 9(b) and 9(d). The measured results are well in accordance with the simulations shown in Fig. 3. Some small fluctuations occur in the z-axis direction, and these are caused by reflections from the ground floor. Other measurement errors may arise from the imperfect positioning of the center of the sphere on the radiation axis of the PAL, as well as the location error of the array microphone and scattering from the microphones and other measurement equipment. It can be observed that the directivity of the audio sound generated by the PAL is severely deteriorated on the back side of the sphere, which is consistent with the simulation conclusions.

Figure 10(a) compares the measured audio SPL with and without the sphere for the microphone located at $x=0.7$ m and $z=-0.7$ m, which is approximately at the azimuthal angle $\theta=135°$ and the radius of 1.0 m to the center of the sphere. Only the results at the center frequencies in the 1/3 octave band from 300 Hz to 4 kHz were measured and plotted. Figure 10(b) compares the SPL increment for simulation and experiment results after introducing the sphere. It can be found the measured results are generally in accordance with the numerical ones. The large mismatches between the simulation and experimental results are observed at high frequencies, which might be because the positioning of the equipment is more sensitive at small wavelengths and the scattering effects of the microphone array become more prominent. It is clear the audio SPL is enlarged after introducing the sphere. Informal hearing tests also showed that a listener in front of the PAL can hear the audio sound scattered back after introducing the sphere as if it is reflected by the sphere. This is different to the perception of the scattered audio sound generated by a conventional loudspeaker.

V. CONCLUSIONS

In this paper, a computationally efficient method is developed to calculate the quasilinear solution of the scattering by a rigid sphere of audio sound generated by a PAL based on both the Kuznetsov and Westervelt equations. The audio SPL calculated using the Westervelt equation is found generally to be larger than that using the Kuznetsov equation because the source density for audio sound calculated using

https://doi.org/10.1121/10.0009750

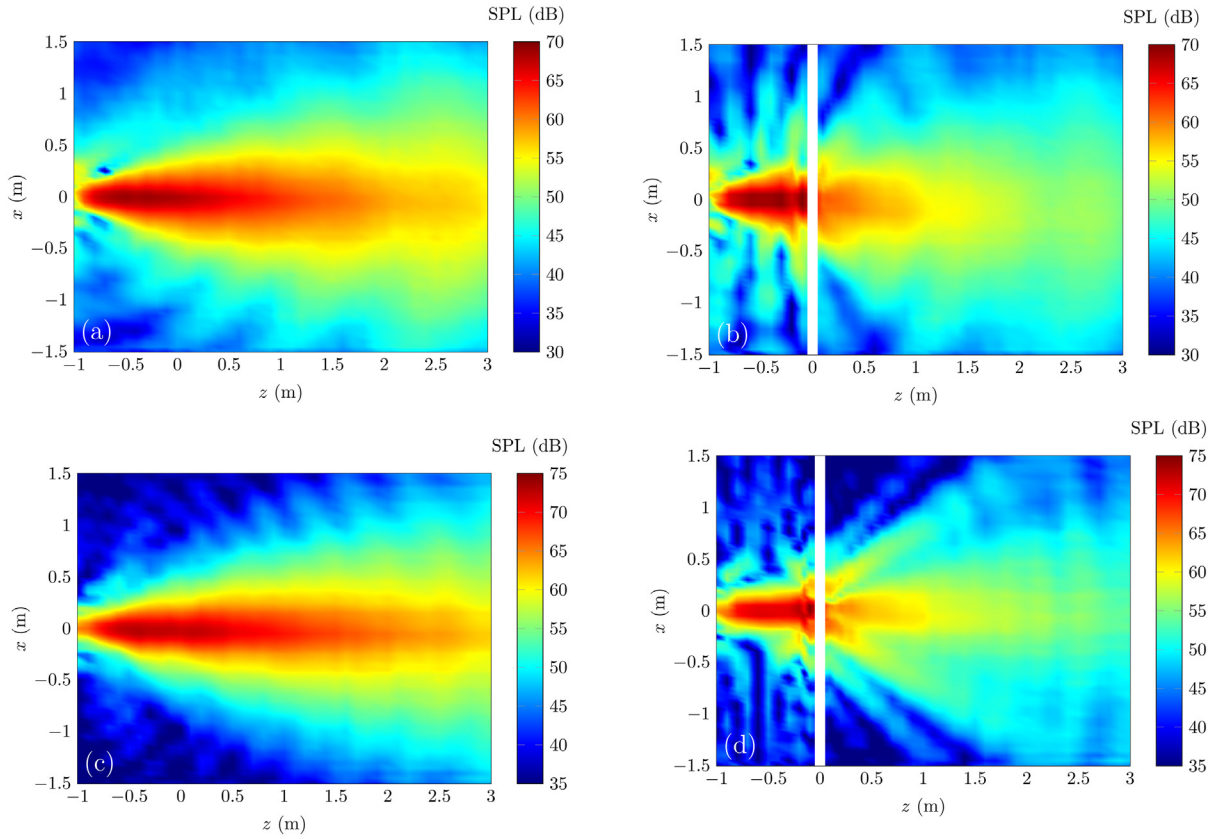

FIG. 9. (Color online) Sound fields generated by a PAL: (a) without the sphere at 1 kHz; (b) with the sphere at 1 kHz; (c) without the sphere at 2 kHz; and (d) with the sphere at 2 kHz.

the Westervelt equation is larger due to the assumption of the two collinear ultrasonic beams. The error using the Westervelt equation is found to be significant, especially at the field points near the sphere at low frequencies, where local effects are strong and cannot be correctly captured by the Westervelt equation.

Both the simulation and experimental results demonstrate that the directivity of the audio sound generated by a PAL severely deteriorates after introducing the sphere. This means a listener behind another listener whose head is on the radiation direction of the PAL cannot expect a highly collimated audio beam as it should be. The reason is that the ultrasounds forming the directivity of the audio sound are almost completely blocked by the sphere. It is also interesting to note that the listener on the front side of a sphere, between the PAL and the sphere, can hear some audio sound as if it is played from the sphere. The reason is that the reflected ultrasounds form another virtual array that augments the audio sound on the front side of the sphere. However, the effects of the sphere for the listener on the front side are negligible for conventional loudspeakers. The physical mechanism accounting for this difference is that the size of the sphere is much larger than the ultrasound wavelength, so it significantly affects the progradation of

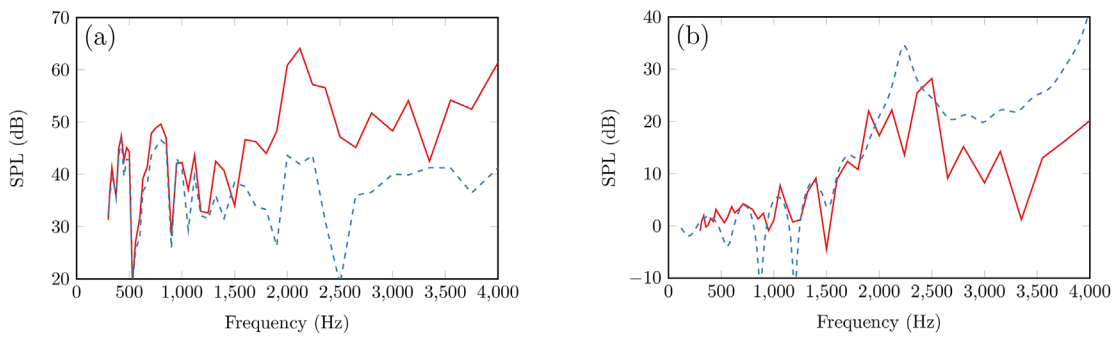

FIG. 10. (Color online) Measured audio sound at the microphone located at $x = 0.7$ m and $z = -0.7$ m generated by a PAL at the frequencies from 300 Hz to 4 kHz: (a) the SPL with (solid line) and without the sphere (dashed line); (b) the SPL increment by experiments (solid line) and simulations (dashed line).

ultrasound waves and consequently influences the behavior of the demodulated audio sound. The methods and results presented in this work provide guidance for analyzing the scattering effects of a human head on personal audio applications using PALs.

It is noted that the boundary condition on the surface of the sphere is assumed to be rigid in this work. When the boundary becomes non-rigid, the radial component of the Green's function given by Eq. (12) should be modified to satisfy the specific boundary condition. The scattered field would then be more complicated, especially for the field between the PAL and the sphere, and this awaits further work. It may also be interesting to investigate the behavior of the audio sound when two or more spheres exist in order to simulate multiple listeners.

ACKNOWLEDGMENTS

This research was supported by the Australian Research Council's Linkage Project funding scheme (LP160100616). H.Z. also gratefully acknowledges the financial support by National Natural Science Foundation of China (11874219).

[1]W.-S. Gan, J. Yang, and T. Kamakura, "A review of parametric acoustic array in air," Appl. Acoust. **73**(12), 1211–1219 (2012).
[2]Y. Nakashima, T. Ohya, and T. Yoshimura, "Prototype of parametric array loudspeaker on mobile phone and its acoustical characteristics," in *Proceedings of the Audio Engineering Society Convention 118*, Barcelona, Spain (May 28–31, 2005), pp. 1–6.
[3]N. Tanaka and M. Tanaka, "Mathematically trivial control of sound using a parametric beam focusing source," J. Acoust. Soc. Am. **129**(1), 165–172 (2011).
[4]Y. Ogami, M. Nakayama, and T. Nishiura, "Virtual sound source construction based on radiation direction control using multiple parametric array loudspeakers," J. Acoust. Soc. Am. **146**(2), 1314–1325 (2019).
[5]B. Castagnède, A. Moussatov, D. Lafarge, and M. Saeid, "Low frequency in situ metrology of absorption and dispersion of sound absorbing porous materials based on high power ultrasonic non-linearly demodulated waves," Appl. Acoust. **69**(7), 634–648 (2008).
[6]M. Arnela, C. Martínez-Suquía, and O. Guasch, "Characterization of an omnidirectional parametric loudspeaker with exponential sine sweeps," Appl. Acoust. **182**, 108268 (2021).
[7]C. Ye, Z. Kuang, P. Ji, and J. Yang, "Generation of audible sound from two ultrasonic beams with dummy head," Jpn. J. Appl. Phys. **47**(5), 4333–4335 (2008).
[8]H. Zou and X. Qiu, "Performance analysis of the virtual sound barrier system with a diffracting sphere," Appl. Acoust. **69**(10), 875–883 (2008).
[9]R. O. Duda and W. L. Martens, "Range dependence of the response of a spherical head model," J. Acoust. Soc. Am. **104**(5), 3048–3058 (1998).
[10]P. J. Westervelt, "Parametric acoustic array," J. Acoust. Soc. Am. **35**(4), 535–537 (1963).
[11]J. Zhong, R. Kirby, and X. Qiu, "The near field, Westervelt far field, and inverse-law far field of the audio sound generated by parametric array loudspeakers," J. Acoust. Soc. Am. **149**(3), 1524–1535 (2021).
[12]S. I. Aanonsen, T. Barkve, J. N. Tjøtta, and S. Tjøtta, "Distortion and harmonic generation in the nearfield of a finite amplitude sound beam," J. Acoust. Soc. Am. **75**(3), 749–768 (1984).
[13]M. Červenka and M. Bednařík, "A versatile computational approach for the numerical modelling of parametric acoustic array," J. Acoust. Soc. Am. **146**(4), 2163–2169 (2019).
[14]M. F. Hamilton and J. A. TenCate, "Sum and difference frequency generation due to noncollinear wave interaction in a rectangular duct," J. Acoust. Soc. Am. **81**(6), 1703–1712 (1987).
[15]M. F. Hamilton and D. T. Blackstock, *Nonlinear Acoustics* (Acoustical Society of America, New York, 2008).
[16]J. Zhong, R. Kirby, and X. Qiu, "A non-paraxial model for the audio sound behind a non-baffled parametric array loudspeaker (L)," J. Acoust. Soc. Am. **147**(3), 1577–1580 (2020).
[17]M. Červenka and M. Bednařík, "Non-paraxial model for a parametric acoustic array," J. Acoust. Soc. Am. **134**(2), 933–938 (2013).
[18]J. Zhong, R. Kirby, and X. Qiu, "A spherical expansion for audio sounds generated by a circular parametric array loudspeaker," J. Acoust. Soc. Am. **147**(5), 3502–3510 (2020).
[19]C. Shi and Y. Kajikawa, "A convolution model for computing the far-field directivity of a parametric loudspeaker array," J. Acoust. Soc. Am. **137**(2), 777–784 (2015).
[20]J. Zhong, S. Wang, R. Kirby, and X. Qiu, "Reflection of audio sounds generated by a parametric array loudspeaker," J. Acoust. Soc. Am. **148**(4), 2327–2336 (2020).
[21]J. Zhong, S. Wang, R. Kirby, and X. Qiu, "Insertion loss of a thin partition for audio sounds generated by a parametric array loudspeaker," J. Acoust. Soc. Am. **148**(1), 226–235 (2020).
[22]L. Tong, S. Lai, J. Yan, and C. Li, "Highly directional acoustic waves generated by a horned parametric acoustic array loudspeaker," J. Vib. Acoust. **141**(1), 011012 (2019).
[23]M. Červenka and M. Bednařík, "Parametric acoustic array lensed by a gradient-index phononic crystal," J. Acoust. Soc. Am. **149**(6), 4534–4542 (2021).
[24]I. B. Abbasov and N. P. Zagrai, "Sphere scattering of nonlinearly interacting acoustic waves," Fluid Dyn. **30**(2), 158–165 (1995).
[25]G. T. Silva and A. Bandeira, "Difference-frequency generation in nonlinear scattering of acoustic waves by a rigid sphere," Ultrasonics **53**(2), 470–478 (2013).
[26]H. E. Bass, L. C. Sutherland, A. J. Zuckerwar, D. T. Blackstock, and D. M. Hester, "Atmospheric absorption of sound: Further developments," J. Acoust. Soc. Am. **97**(1), 680–683 (1995).
[27]Y. Kagawa, T. Tsuchiya, T. Yamabuchi, H. Kawabe, and T. Fujii, "Finite element simulation of non-linear sound wave propagation," J. Sound Vib. **154**(1), 125–145 (1992).
[28]G. Gaunaurd, H. Huang, and H. Strifors, "Acoustic scattering by a pair of spheres," J. Acoust. Soc. Am. **98**(1), 495–507 (1995).
[29]Z. Lin, J. Lu, C. Shen, X. Qiu, and B. Xu, "Active control of radiation from a piston set in a rigid sphere," J. Acoust. Soc. Am. **115**(6), 2954–2963 (2004).
[30]H. Zou, X. Qiu, J. Lu, and F. Niu, "A preliminary experimental study on virtual sound barrier system," J. Sound Vib. **307**(1–2), 379–385 (2007).
[31]J. J. Bowman, T. B. Senior, and P. L. Uslenghi, *Electromagnetic and Acoustic Scattering by Simple Shapes* (North-Holland Publishing Company, Amsterdam, the Netherlands, 1970).
[32]S. Zhang and J. Jin, *Computation of Special Functions* (John Wiley & Sons, New York, 1996).
[33]T. D. Mast and F. Yu, "Simplified expansions for radiation from a baffled circular piston," J. Acoust. Soc. Am. **118**(6), 3457–3464 (2005).
[34]J. Zhong and X. Qiu, "On the spherical expansion for calculating the sound radiated by a baffled circular piston," J. Theor. Comput. Acoust. **28**, 2050026 (2020).
[35]M. Majić and E. C. Le Ru, "Numerically stable formulation of Mie theory for an emitter close to a sphere," Appl. Opt. **59**(5), 1293–1300 (2020).
[36]ISO 9613-1:1993: *Acoustics — Attenuation of Sound during Propagation Outdoors — Part 1: Calculation of the Absorption of Sound by the Atmosphere* (International Organization for Standardization, Genève, Switzerland, 1993).
[37]P. Ji and J. Yang, "An experimental investigation about parameters' effects on spurious sound in parametric loudspeaker," Appl. Acoust. **148**, 67–74 (2019).